Downloaded by UNIV OF CALIFORNIA BERKELEY at 15:29:47:886 on June 11, 2019
from https://pubs.acs.org/doi/10.1021/nn501481u.

ARTICLE

Nanopillar Lasers Directly Grown on Silicon with Heterostructure Surface Passivation

Hao Sun,[†,‡] Fan Ren,[†] Kar Wei Ng,[†] Thai-Truong D. Tran,[†] Kun Li,[†] and Connie J. Chang-Hasnain[†,*]

[†]Department of Electrical Engineering and Computer Sciences, University of California at Berkeley, Berkeley, California 94720, United States, and [‡]Department of Electronic Engineering, Tsinghua University, Beijing, 100084, People's Republic of China

ABSTRACT

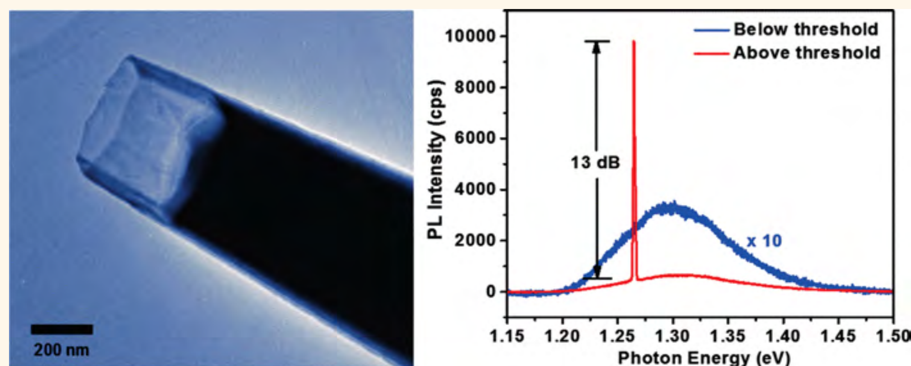

Single-crystalline wurtzite InGaAs/InGaP nanopillars directly grown on a lattice-mismatched silicon substrate are demonstrated. The nanopillar growth is in a core—shell manner and gives a sharp, defect-free heterostructure interface. The InGaP shell provides excellent surface passivation effect for InGaAs nanopillars, as attested by 50-times stronger photoluminescence intensities and 5-times greater enhancements in the carrier recombination lifetimes, compared to the unpassivated ones. A record value of 16.8% internal quantum efficiency for InGaAs-based nanopillars was attained with a 50-nm-thick InGaP passivation layer. A room-temperature optically pumped laser was achieved from single, as-grown InGaAs nanopillars on silicon with a record-low threshold. Superior material qualities of these InGaP-passivated InGaAs nanopillars indicate the possibility of realizing high-performance optoelectronic devices for photovoltaics, optical communication, semiconductor nanophotonics, and heterogeneous integration of III—V materials on silicon.

KEYWORDS: core—shell · nanopillars · nanowires · surface passivation · lasers · III—V compound on Si

GaAs-based materials are prevalent in the optoelectronics industry, with extensive deployments in semiconductor lasers, photovoltaics, and high-frequency electronics.[1−4] The highest conversion efficiencies of single-junction solar cells are also attained with GaAs-based material,[5−7] as it exhibits a direct band gap and large absorption coefficient. However, the high cost of GaAs substrates is well recognized as one of the most critical issues to the wide development of these materials. There have been many recent successes in direct growth of GaAs-based nanostructures on silicon substrates, which can greatly reduce substrate costs.[8−11] Another major challenge to realize high-performance GaAs-based devices lies in its high surface recombination velocity (SRV). It was reported that the SRV of GaAs is ~1000 times higher than InP-based material.[12,13] This problem becomes more detrimental for nanostructures, which are more vulnerable compared to thin film bulk materials, due to the significantly higher surface-to-volume ratios directly resulting in low internal quantum yields. The performances of GaAs-based nanostructure devices have so far been inferior to those of planar counterparts.[2,7] Therefore, it is extremely necessary to passivate the surface states of nanostructures to enhance device performances.

There has been intense research on surface passivation techniques to increase photo/electroluminescence intensity using

* Address correspondence to cch@berkeley.edu.

Received for review March 17, 2014 and accepted June 3, 2014.

Published online June 03, 2014
10.1021/nn501481u

© 2014 American Chemical Society

AlGaAs, GaAsP, or InGaP as a surface passivation layer for GaAs-based nanostructures, between which lattice constants are nearly matched.[8−10,14−16] However, most of the investigations focused on nanowires grown on native GaAs substrate.[14−16] In addition, there is a lack of detailed study of material qualities with different surface passivation materials, structures, and dimensions. All these parameters ultimately contribute to the device performances with such complex heterostructures in nanoscale dimensions. Thus, it is particularly important and meaningful to gain some insight into the physical properties, in order to accelerate the employment of novel nanostructures into optoelectronic devices, such as nanolasers and solar cells.

Recently, we reported a new metastable growth mode of InGaAs/GaAs core−shell nanopillar lasers grown directly on a silicon substrate using low-temperature metal−organic chemical vapor deposition (MOCVD).[17−19] This catalyst-free growth mechanism produces self-assembled, single-crystalline wurtzite-phased material with very high crystal quality and growth controllability. The core−shell growth allows for scaling the pillar diameters from nanometer to micrometer dimensions while still preserving the single-crystalline wurtzite phase, despite the large lattice mismatch with the silicon substrate.[20] This alleviates the large surface-to-volume ratio constraint that nanowires commonly suffer from. It also enables the formation of a great range of radial heterostructures and quantum wells.[21] Most importantly, the radial heterostructures become more tolerant to lattice mismatch, since the three-dimensional geometry and small size allow for efficient elastic strain relaxation.[22] In addition, the catalyst-free growth and the low growth temperature between 400 and 450 °C make this growth method very promising for monolithic integration of III−V nanolasers on silicon with the standard CMOS process.[18] However, despite of all the advantages discussed above, the internal quantum efficiency (IQE) for GaAs-passivated InGaAs pillars is still quite low, making it a major deficiency for device applications.

In this work, we report InGaP-passivated InGaAs nanopillar lasers grown directly on a silicon substrate. High-quality single-crystalline wurtzite InGaAs/InGaP material as well as defect-free heterostructure interfaces were successfully demonstrated. We prove that InGaP is more effective than GaAs as surface passivation material for InGaAs nanopillars, as attested by the following observations. The InGaP-passivated InGaAs structure shows up to 50-times boost in photoluminescence (PL) intensities and 5-times enhancement in the carrier recombination lifetimes, compared to the unpassivated nanopillars. These improvements are attributed to a larger band offset between InGaP/InGaAs acting as a barrier to prevent carriers from reaching and recombining at the surface. A significant improvement on IQE of 16.8% was attained at high excitation levels, compared with only ~3% from GaAs- or AlGaAs-passivated pillars. Room-temperature lasing oscillation from single as-grown nanopillars was achieved with a very low threshold under optical pumping. These superior optical properties of wurtzite InGaAs/InGaP heterostructure nanopillars on silicon would significantly broaden the range of applications for nanostructures.

RESULTS AND DISCUSSION

Core−Shell InGaAs/InGaP Nanopillars in Wurtzite Phase. Catalyst-free, defect-free single-crystalline wurtzite InGaAs/InGaP nanopillars are directly grown on silicon substrates. The smooth surface morphology of a typical nanopillar grown vertically on a (111)-Si substrate is shown in a side-view scanning electron microscopy (SEM) image (Figure 1a). The nanopillars have well-faceted hexagonal cross sections (Figure 1b), which originate from the wurtzite crystalline phase. To further prove the core−shell growth mode, wet chemical etching was used to selectively etch away the InGaAs core, resulting in a thin InGaP layer at the tip. Excellent InGaP shell layer growth can be clearly seen from the semitranslucent portion in the transmission electron microscopy (TEM) image (Figure 1c). A high-angle annular dark field scanning transmission electron microscopy (HAADF-STEM) image of a pillar with a nominal ~150-nm-thick shell is illustrated in Figure 1d. The thickness of InGaP shell agrees well with the designed value, as indicated by the scale bar. To study the heterointerface quality, a high-resolution TEM (HRTEM) study was performed at the exact InGaAs/InGaP interface (Figure1e). The crystal continues as a coherent wurtzite phase across the heterostructure interface. Figure 1f is the HRTEM image inside the InGaP portion, far away from the heterointerface. The corresponding selected area diffraction pattern (SADP) recorded along the zone axis is shown in Figure 1g. Both the characteristic zigzag lattice arrangement and clear distinctive diffraction pattern confirm that the nanopillars are in single-crystalline wurtzite phase. Figure 1h is a low-magnification side-view SEM image of an array of InGaAs/InGaP nanopillars. With 92 min growth time, the pillars have a base diameter of ~675 ± 50 nm and a length of ~3.5 ± 0.7 μm. The variation of the pillar diameter is quite small, whereas that of the pillar length is relatively large. Since the dimension of the pillars varies, all of the following optical photoluminescence studies are average values among more than 10 pillars with similar dimensions verified by SEM images.

Optical Properties of InGaAs Pillars with Different Passivation Materials. The effectiveness of InGaP passivation layers for InGaAs nanopillars is studied by comparing nanopillars with three different passivation materials while keeping the same InGaAs core diameter of ~600 nm. The three samples are unpassivated-InGaAs (bare-InGaAs),

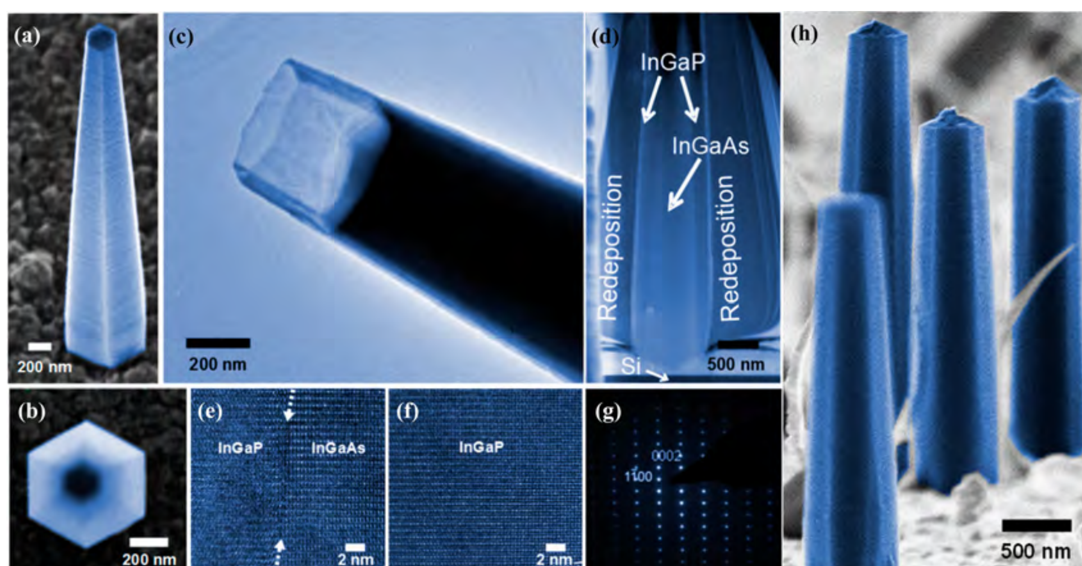

Figure 1. (a) Tilt-view (30°) SEM image of a typical InGaAs/InGaP nanopillar grown vertically on a (111)-Si substrate with smooth surfaces. (b) Top-view SEM image of the nanopillar with a well-faceted hexagonal cross-section, which originates from the wurtzite crystal phase. (c) TEM image of a semitranslucent pillar tip after selective etching away the InGaAs core, which proves the core−shell growth mode. (d) HAADF-STEM image of a nanopillar with a nominal ~150-nm-thick InGaP shell. A thick silicon redeposition layer is observed wrapping around the nanopillar as a result of sample preparation by focused ion beam milling. The pillar tip was damaged during ion milling. (e) HRTEM image at the exact InGaAs/InGaP interface. The crystal continues as a coherent wurtzite phase across the heterostructure. (f) HRTEM image inside the InGaP portion far away from the heterointerface. (g) Clear SADP image recorded along the (11$\bar{2}$0) zone axis. Both the characteristic zigzag lattice arrangement and clear distinctive diffraction pattern confirm that the nanopillars are in the single-crystalline wurtzite phase. (h) Tilt-view (80°) SEM image of an array of InGaAs/InGaP nanopillars with 92 min growth time. The pillars have a base diameter of ~675 ± 50 nm and a length of ~3.5 ± 0.7 μm.

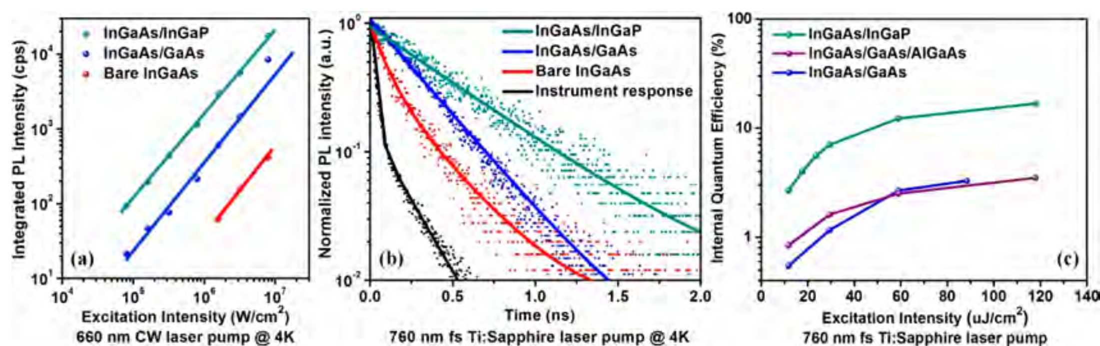

Figure 2. (a) Integrated PL intensity *versus* excitation intensity in logarithmic scale with linear curve fit at 4 K for bare-InGaAs pillar (red), GaAs-passivated pillar (blue), and InGaP-passivated pillar (green). The PL intensity is enhanced by ~10 and ~50 times for InGaAs nanopillars with GaAs and InGaP passivation layers, respectively. (b) Corresponding TRPL decay curves measured at 4 K. The dots represent raw experimental data, and the solid lines are the fitting results with exponential decay functions. The black curve represents the system instrument response of ~40 ps. The effective carrier lifetimes are ~90 ps (red), ~293 ps (blue), and ~492 ps (green), respectively. (c) IQE values extracted from the ratio of integrated PL intensity from 298 and 4 K, as a function of excitation intensities for three types of structures: InGaAs/GaAs (blue), InGaAs/GaAs/AlGaAs core−shell−cap (purple), and InGaAs/InGaP (green). The IQE value of InGaAs/InGaP nanopillars at high excitation level is 16.8%, while only ~3% for the other two structures.

GaAs-passivated, and InGaP-passivated InGaAs nanopillars. Figure 2a shows the integrated PL intensity trends of different nanopillars as a function of excitation intensity by using a continuous wave (CW) laser source at 4 K. The fewer number of data points for the bare-InGaAs pillar is limited by detection sensitivity due to its low PL emission intensity. The PL intensity is enhanced by ~10 and ~50 times for nanopillars with GaAs and InGaP passivation layers, respectively. Representative 4 K time-resolved photoluminescence (TRPL) decay curves of the three samples are recorded at the peak emission energy, as shown in Figure 2b. It is shown that the effective carrier lifetime of unpassivated-InGaAs nanopillars is approximately 90 ps, nearly reaching the instrument response time. The GaAs-passivated InGaAs nanopillars exhibit a slightly longer lifetime of ~293 ps, benefiting from the passivation of surface states. The carrier lifetime of InGaAs/InGaP pillars is ~492 ps, enhanced by a factor of 5 compared to the unpassivated ones. This improvement is

attributed to a larger band offset between the cladding InGaP layer and the active InGaAs core compared to that of the InGaAs/GaAs structure. The band gap of the InGaP shell was determined by growing pure InGaP nanopillars on silicon with the same growth conditions and chemical stoichiometry. Strong photoluminescence was obtained showing direct band gap emission at ~1.47 eV at room temperature.[23] This wider band gap InGaP material could act as a barrier to prevent carriers from reaching and recombining at the surface, which effectively prohibits the carrier recombination. The absence of misfit dislocation defects at the InGaAs/InGaP heterointerface also contributes to the enhancement of optical properties. Therefore, we conclude that the effective surface passivation of the InGaP shell, together with the high material quality, contributes to the PL intensity and lifetime enhancement.

To further explore the feasibility of using InGaP-passivated InGaAs nanopillars for high-performance optoelectronic applications, IQE measurements were carried out. IQE is a critical figure-of-merit to evaluate the performance of optoelectronic devices, such as solar cells and light-emitting diodes. This parameter is usually very low in nanowire-based devices, due to the high surface recombination velocities. IQE values can be extracted from the ratio of integrated PL intensity under room temperature and 4 K, assuming 100% of IQE at 4 K.[24−26] These measurements are based on the assumption that nonradiative recombination can be neglected at low temperatures. It should be noted that this is not necessarily the case, and the values found using this method represent an upper limit for the IQE. The IQE value, *i.e.*, the ratio of integrated PL intensities from 298 and 4 K, *versus* excitation intensity of single nanopillars from three samples is shown in Figure 2c. The samples are InGaAs/InGaP, InGaAs/GaAs/AlGaAs core−shell−cap, and InGaAs/GaAs structures, respectively. As can be seen, the IQE value is strongly dependent on the excitation intensity. At low excitation levels, with such high surface-to-volume ratio of the nanostructures, the nonradiative recombination mechanism dominates. At high excitation levels, for GaAs-passivated InGaAs pillars, the best IQE value is only ~3%. Adding an AlGaAs capping layer to the InGaAs/GaAs pillar does not lead to significant improvement of the IQE value. This could be because that aluminum is known to get oxidized very easily and shows a strong propensity toward the formation of oxygen-related deep-level defects, which then can act as recombination centers at the GaAs/AlGaAs interface.[27,28] Significant IQE enhancement was achieved with an InGaP passivation layer, leading to an IQE value of 16.8%, which is significantly higher than the IQE value obtained from GaAs/InGaP nanowires grown on silicon reported previously.[26] In that paper, the authors attributed the low efficiency value to the misfit strains generated at the GaAs/InGaP heterointerface and the rotational twins due to the large lattice mismatch with the substrate.

Reducing the crystal lattice strain between the InGaAs core and the radially grown InGaP shell is very important for improving the interface quality and optical performance. In this work, a series of InGaAs/InGaP nanopillars were grown to optimize the growth parameters by tuning the trimethylindium (TMIn) to triethylgallium (TEGa) ratio. The chemical stoichiometry of the core is $In_{0.12}Ga_{0.88}As$, determined from both PL peak energy and flow rate ratio of the gas precursors. However, accurately determining the chemical composition of the InGaP shell is rather difficult. The chemical stoichiometry of the InGaP shell layer was estimated from the flow rate ratio of group III precursors. The results we demonstrated here are from growth conditions with optimized InGaP composition. Although there is most likely a lattice mismatch between the InGaAs core and InGaP shell, the nanopillars exhibit single-crystalline wurtzite phase through the entire pillar, benefiting from the core−shell growth mode.[20,22] Polytypism is confined only 200−400 nm at the root of the nanopillar and horizontally terminated at the sidewall. Furthermore, we didn't observe any misfit dislocations or rotational twins at the heterointerface, as shown in Figure 1. Another fact is that the submicrometer-sized structures we demonstrated here greatly reduce the surface-to-volume ratio. Excellent material quality, together with uniform morphological property are believed to contribute to this high IQE value. The IQE results shown here also suggest that InGaP-passivated InGaAs nanopillars could be indeed a promising material system for high-performance nanophotonic devices compared to InGaAs/GaAs. Thus, we will focus on the InGaAs/InGaP nanopillars in the following studies by optimizing structure dimensions in order to select the best structures for device applications.

Optical Properties of InGaAs/InGaP Pillars with Various Dimensions. To understand how InGaP shell thicknesses play a role in these nanopillar structures, a variety of samples with nominal 25- to 200-nm-thick InGaP shells were studied. Figure 3a shows the integrated PL intensity trends of InGaAs/InGaP nanopillars with different InGaP layer thicknesses at 4 K. No prominent variation in the PL intensities was observed among the samples with thicker shells, which indicates that 25−50-nm-thick InGaP could already provide effective passivation to inhibit carrier recombination at the pillar surface. It is well understood that by increasing the pillars' dimensions, the surface-to-volume ratio can be reduced, which directly leads to the suppression of nonradiative recombination. Up to 10 times enhancement was attained at low excitation levels by increasing the InGaAs core diameter from ~600 nm to ~900 nm (Figure 3b). No significant increase was observed at high excitation levels, which is probably

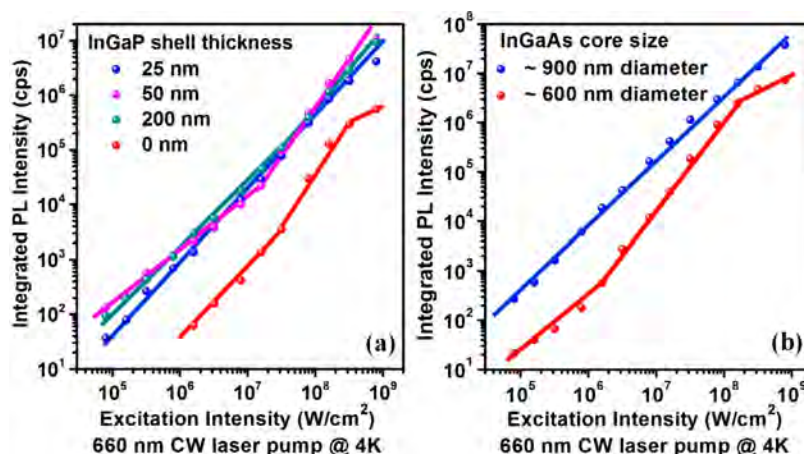

Figure 3. (a) Integrated PL intensity *versus* excitation intensity in logarithmic scale with linear curve fit at 4 K from samples with different InGaP thinknesses: 0 nm (bare-InGaAs pillars, red), 25 nm (blue), 50 nm (pink), and 200 nm (green). No prominent variation in the PL intensities was observed among the samples with thicker shells. (b) Same plot from samples with different InGaAs core diameters: ~600 nm (red) and ~900 nm (blue). Up to 10-times enhancement was attained at low excitation levels by increasing the InGaAs core diameter from ~600 nm to ~900 nm. The InGaP layers in this study are ~50 nm in thicknesses.

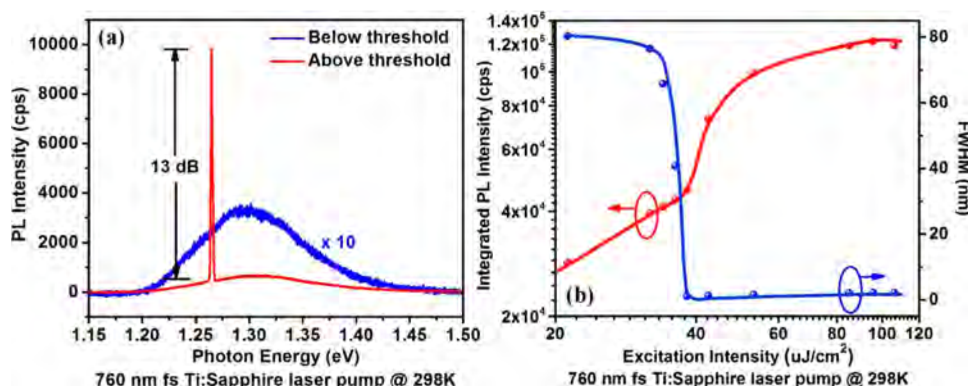

Figure 4. (a) PL emission and lasing spectra at 298 K from a single as-grown nanopillar below and above lasing threshold. Below threshold, broad spontaneous emission is observed. The blue curve has been multiplied by 10 times for visibility. A strong lasing peak dominates emission above threshold with a sideband suppression ratio of ~13 dB. (b) Corresponding PL intensity and line width (fwhm) plotted as a function of excitation intensity. The line width decreases by a factor of ~80 near and above the lasing threshold. A clear lasing threshold is observed at 38.2 μJ/cm^2, which is significantly lower than the result from transferred GaAs-based nanowire lasers published recently.

due to the saturation of surface states, leading to a higher possibility for carriers to recombine radiatively. Since the dimension of the InGaAs pillars is scalable with growth time, we believe optimization of the growth condition to achieve micrometer-sized pillars would further improve the optical property thus device performance.

Low-Threshold Room-Temperature Lasing from Single As-Grown Nanopillars. Finally, we demonstrated optically pumped single as-grown nanopillar lasers at room temperature. To our best knowledge, no room-temperature lasing operation has been achieved thus far for as-grown unpassivated-InGaAs nanopillars.[14,17,29,30] This further proves that InGaP is sufficient passivation material that facilitates good carrier confinement in the InGaAs core. Room-temperature PL emission spectra from a single as-grown nanopillar below and above the lasing threshold are shown in Figure 4a. Below threshold, broad spontaneous emission is observed. A strong lasing peak dominates emission above threshold with a sideband suppression ratio of ~13 dB. The corresponding PL intensity and line width at full width at half-maximum (fwhm) as a function of excitation intensity are plotted in Figure 4b. A clear lasing threshold is observed at 38.2 μJ/cm^2. The pump fluence value to achieve lasing is significantly lower than the result from transferred GaAs/AlGaAs and GaAs/AlGaAs/GaAs core–shell–cap nanowire lasers published recently[29,30] and about two times lower compared with InGaAs/GaAs nanopillar lasers we demonstrated before.[17] The lasing with ultralow threshold excitation intensity in the InGaP-passivated structure is attributable to the sufficient reduction of nonradiative recombination as discussed above.

CONCLUSIONS

In summary, we demonstrate the catalyst-free MOCVD growth of InGaAs/InGaP core−shell nanopillars with single-crystalline wurtzite phase at a low temperature. Despite the large lattice mismatch between nanopillar and silicon substrate, both defect-free InGaAs and InGaP layers as well as high crystal quality heterointerfaces are achieved. PL emission intensity of InGaAs pillars was boosted by up to 50 times *via* InGaP passivation. A record value of 16.8% IQE was achieved from InGaAs/InGaP pillars at high excitation levels, compared with ∼3% for GaAs/AlGaAs-passivated InGaAs pillars. By increasing the pillar diameters from ∼600 nm to ∼900 nm, another 10-times increment in PL intensity was obtained. No obvious trends in PL intensities were observed with increasing InGaP shell thickness from 25 to 200 nm. Furthermore, optically pumped lasing from single as-grown nanopillars was attained at room temperature with the lowest reported threshold for GaAs-based nanowire/nanopillar lasers. Therefore, the outperformed InGaAs/InGaP nanopillars directly grown on silicon could fulfill a potential for heterogeneous integration, optical communication, and optoelectronic devices with low cost and improved performance. These observations would open up future opportunities to design novel nanophotonic architectures.

MATERIALS AND METHODS

Nanopillar Synthesis. Trimethylindium (TMIn), triethylgallium (TEGa), tertiarybutylarsine (TBAs), and tertiarybutylphosphine (TBP) were used as indium, gallium, arsenic, and phosphorus precursors, respectively. The growth started with an InGaAs core at 400 °C, followed by a uniform surrounding epitaxial InGaP layer at 450 °C. The input V/III ratio of the InGaAs core was set as 50, and the whole epitaxial process was catalyst-free. Since nanopillar growth follows a metastable core−shell manner, the radius or thickness of each portion is controllable and nearly linearly scalable with the corresponding growth time. The base diameter of InGaAs cores was designed as 600 or 900 nm. The thicknesses of the InGaP capping layer were designed as 25, 50, 150, and 200 nm in the present paper.

Electron Microscopy. HRTEM and HAADF-STEM studies were carried out in a FEI Titan transmission electron aberration-corrected microscope operating at 300 keV. Sample preparation involves the extraction of a lamella from an as-grown nanopillar with the use of focused ion beam milling and *in situ* micromanipulations. Pt is deposited on the area of interest to anchor the loose needle onto the substrate and provide passivation against ion damage. The lamella was then further thinned down to electron transparent thickness with an argon ion beam.

Optical Spectroscopy. Micro-PL measurements were carried out in a continuous-flow liquid-helium cryostat with a CW laser diode at 660 nm. TRPL measurements were performed with a mode-locked Ti:sapphire femtosecond laser at 760 nm. The laser spot was focused down to a ∼5-μm-diameter spot through an NIR-optimized 100× microscope objective. PL signal was collected *via* the same objective and dispersed through a spectrometer with a liquid-nitrogen-cooled silicon CCD. Additional long-pass filters were employed to prevent exposing the detection system to high laser power. PL decay traces were obtained by using the time-correlated single photon counting method in conjunction with a silicon avalanche photodiode for detection. The time resolution of the instrument system was ∼40 ps.

Conflict of Interest: The authors declare no competing financial interest.

Acknowledgment. This work was supported by U.S. DOE SunShot DE-EE0005316, DoD NSSEFF Fellowships N00244-09-1-0013 and N00244-09-1-0080, NSF Award 0939514, California Advanced Solar Technologies Institute, UC Multicampus Research Program and Initiatives (MRPI), and the Alexander von Humboldt Research Award. The authors acknowledge the support of the National Center for Electron Microscopy (NCEM), Lawrence Berkeley Laboratory, which is supported by the U.S. DOE under Contract No. DE-AC02-05CH11231.

REFERENCES AND NOTES

1. Ma, K.; Urata, R.; Miller, D. A. B.; Harris, J. S. Low-Temperature Growth of GaAs on Si Used for Ultrafast Photoconductive Switches. *IEEE J. Quantum Electron.* **2004**, *40*, 800–804.
2. Liang, D.; Kang, Y.; Huo, Y.; Chen, Y.; Cui, Y.; Harris, J. S. High-Efficiency Nanostructured Window GaAs Solar Cells. *Nano Lett.* **2013**, *13*, 4850–4856.
3. Picqué, J. L.; Roizen, S. Frequency-Controlled CW Tunable GaAs Laser. *Appl. Phys. Lett.* **1975**, *27*, 340.
4. Whitbread, N. D.; Edge, C.; Gibson, M.; Wale, M. J. GaAs/AlGaAs Photonics Integrated Circuit for Optical Beam-forming in Phased Array Communication Antennas. *Proc. SPIE* **2000**, 66–74.
5. Green, M. A.; Emery, K.; Hishikawa, Y.; Warta, W.; Dunlop, E. D. Solar Cell Efficiency Tables (version 42). *Prog. Photovolt: Res. Appl.* **2013**, *21*, 827–837.
6. Bauhuis, G. J.; Mulder, P.; Haverkamp, E. J.; Huijben, J. C. C. M.; Schermer, J. J. 26.1% Thin Film GaAs Solar Cell Using Epitaxial Lift-Off. *Sol. Energy Mater. Sol. Cells* **2009**, *93*, 1488–1491.
7. Kayes, B. M.; Nie, H.; Twist, R.; Spruytte, S. G.; Reinhardt, F.; Kizilyalli, I. C.; Higashi, G. S. 27.6% Conversion Efficiency, A New Record for Single-Junction Solar Cells under 1 Sun Illumination. *37th IEEE Photovoltaic Specialists Conference (PVSC)* **2011**, 000004–000008.
8. Breuer, S.; Pfüller, C.; Flissikowski, T.; Brandt, O.; Grahn, H. T.; Geelhaar, L.; Riechert, H. Suitability of Au- and Self-Assisted GaAs Nanowires for Optoelectronic Applications. *Nano Lett.* **2011**, *11*, 1276–1279.
9. Chang, C. C.; Chi, C.Y.; Yao, M.; Huang, N.; Chen, C. C.; Theiss, J.; Bushmaker, A. W.; LaLumondiere, S.; Yeh, T. W.; Povinelli, M. L.; *et al.* Electrical and Optical Characterization of Surface Passivation in GaAs Nanowires. *Nano Lett.* **2012**, *12*, 4484–4489.
10. Tomioka, K.; Motohisa, J.; Hara, S.; Hiruma, K.; Fukui, T. GaAs/AlGaAs Core Multishell Nanowire-Based Light-Emitting Diodes on Si. *Nano Lett.* **2010**, *10*, 1639–1644.
11. Holm, J. V.; Jørgensen, H. I.; Krogstrup, P.; Nygård, J.; Liu, H.; Aagesen, M. Surface-Passivated GaAsP Single-Nanowire Solar Cells Exceeding 10% Efficiency Grown on Silicon. *Nat. Commun.* **2013**, *4*, 1498.
12. Lloyd-Hughes, J.; Merchant, S. K. E.; Fu, L.; Tan, H. H.; Jagadish, C.; Castro-Camus, E.; Johnston, M. B. Influence of Surface Passivation on Ultrafast Carrier Dynamics and Terahertz Radiation Generation in GaAs. *Appl. Phys. Lett.* **2006**, *89*, 232102.
13. Nelson, R.J.; Sobers, R. G. Minority-Carrier Lifetime and Internal Quantum Efficiency of Surface-Free GaAs. *J. Appl. Phys.* **1978**, *49*, 6103.
14. Hua, B.; Motohisa, J.; Kobayashi, Y.; Hara, S.; Fukui, T. Single GaAs/GaAsP Coaxial Core-Shell Nanowire Lasers. *Nano Lett.* **2009**, *9*, 112–116.

15. Mariani, G.; Scofield, A. C.; Hung, C. H.; Huffaker, D. L. GaAs Nanopillar-Array Solar Cells Employing *in Situ* Surface Passivation. *Nat. Commun.* **2013**, *4*, 1497.
16. Nakai, E.; Yoshimura, M.; Tomioka, K.; Fukui, T. GaAs/InGaP Core-Multishell Nanowire-Array-Based Solar Cells. *Jpn. J. Appl. Phys.* **2013**, *52*, 055002.
17. Chen, R.; Tran, T. T. D.; Ng, K. W.; Ko, W. S.; Chuang, L. C.; Sedgwick, F. G.; Chang-Hasnain, C. J. Nanolasers Grown on Silicon. *Nat. Photonics* **2011**, *5*, 170–175.
18. Lu, F.; Tran, T. T. D.; Ko, W. S.; Ng, K. W.; Chen, R.; Chang-Hasnain, C. Nanolaser Grown on Silicon-Based MOSFETs. *Opt. Express* **2012**, *20*, 12171.
19. Chuang, L. C.; Sedgwick, F. G.; Chen, R.; Ko, W. S.; Moewe, M.; Ng, K. W.; Tran, T. T. D.; Chang-Hasnain, C. J. GaAs-Based Nanoneedle Light Emitting Diode and Avalanche Photodiode Monolithically Integrated on a Silicon Substrate. *Nano Lett.* **2011**, *11*, 385–390.
20. Ng, K. W.; Ko, W. S.; Tran, T. T. D.; Chen, R.; Nazarenko, M. V.; Lu, F.; Dubrovskii, V. G.; Kamp, M.; Forchel, A.; Chang-Hasnain, C. J. Unconventional Growth Mechanism for Monolithic Integration of III-V on Silicon. *ACS Nano* **2013**, *7* (1), 100–107.
21. Ren, F.; Ng, K. W.; Li, K.; Sun, H.; Chang-Hasnain, C. J. High-Quality InP Nanoneedles Grown on Silicon. *Appl. Phys. Lett.* **2013**, *102*, 012115.
22. Nazarenko, M. V.; Sibirev, N. V.; Ng, K. W.; Ren, F.; Ko, W. S.; Dubrovskii, V. G.; Chang-Hasnain, C. J. Elastic Energy Relaxation and Critical Thickness for Plastic Deformation in the Core-Shell InGaAs/GaAs Nanopillars. *J. Appl. Phys.* **2013**, *113*, 104311.
23. Sun, H.; Ren, F.; Tran, T. T. D.; Ng, K. W.; Li, K.; Chang-Hasnain, C. J. High Quality InGaP Micropillars Directly Grown on Silicon, *IEEE Summer Topicals*; Waikoloa, HI, July 8−10, **2013**; paper WA1.2.
24. Jahangir, S.; Banerjee, A.; Bhattacharya, P. Carrier Lifetimes in Green Emitting InGaN/GaN Disks-in-Nanowire and Characteristics of Green Light Emitting Diodes. *Phys. Status Solidi C* **2013**, *10* (No. 5), 812–815.
25. Watanabe, S.; Yamada, N.; Nagashima, M.; Ueki, Y.; Sasaki, C.; Yamada, Y.; Taguchi, T.; Tadatomo, K.; Okagawa, H.; Kudo, H. Internal Quantum Efficiency of Highly-Efficient $In_xGa_{1-x}N$-Based Near-Ultraviolet Light-Emitting Diodes. *Appl. Phys. Lett.* **2003**, *83*, 4906.
26. Svensson, C. P. T.; Mårtensson, T.; Trägårdh, J.; Larsson, C.; Rask, M.; Hessman, D.; Samuelson, L.; Ohlsson, J. Monolithic GaAs/InGaP Nanowire Light Emitting Diodes on Silicon. *Nanotechnology* **2008**, *19*, 305201.
27. Amano, C.; Ando, K.; Yamaguchi, M. The Effect of Oxygen on the Properties of AlGaAs Solar Cells Grown by Molecular Beam Epitaxy. *J. Appl. Phys.* **1988**, *63*, 2853.
28. Tsai, K. L.; Lee, C. P.; Chang, K. H.; Chen, H. R.; Tsang, J. S. Influence of Oxygen on the Performance of GaAs/AlGaAs Quantum Well Infrared Photodetectors. *J. Appl. Phys.* **1994**, *76* (1), 1.
29. Saxena, D.; Mokkapati, S.; Parkinson, P.; Jiang, N.; Gao, Q.; Tan, H. H.; Jagadish, C. Optically Pumped Room-Temperature GaAs Nanowire Lasers. *Nat. Photonics* **2013**, *7*, 963–968.
30. Mayer, B.; Rudolph, D.; Schnell, J.; Morkötter, S.; Winnerl, J.; Treu, J.; Müller, K.; Bracher, G.; Abstreiter, G.; Koblmüller, G.; Finley, J. J. Lasing from Individual GaAs-AlGaAs Core-Shell Nanowires up to Room Temperature. *Nat. Commun.* **2013**, *4*, 2931.